Development of a high-resolution fat and CSF-suppressed optic nerve DTI protocol at 3T: application in multiple sclerosis

Rebecca S. Samson, PhD[a]
Madhan Kolappan, PhD[a]
David L. Thomas, PhD[b]
Mark R. Symms, PhD[c]
Peter Connick, PhD[d]
David H. Miller, MD[a]
Claudia A.M. Wheeler-Kingshott, PhD[a]

[a] NMR Research Unit, Queen Square MS Centre, Department of Neuroinflammation, UCL Institute of Neurology, London, UK
[b] Neuroradiological Academic Unit, Department of Brain Repair and Rehabilitation, UCL Institute of Neurology, London, UK
[c] Department of Clinical & Experimental Epilepsy, UCL Institute of Neurology, London, UK
[d] Department of Clinical Neurosciences, School of Clinical Medicine, University of Cambridge, Addenbrooke's Hospital, Cambridge, UK

Correspondence to: Rebecca Samson
E-mail: r.samson@ucl.ac.uk

Summary

Clinical trials of neuroprotective interventions in multiple sclerosis require outcome measures that reflect the disease pathology. Measures of neuroaxonal integrity in the anterior visual pathways are of particular interest in this context, however imaging of the optic nerve is technically challenging. We therefore developed a 3T optic nerve diffusion tensor imaging protocol incorporating fat and cerebrospinal fluid suppression and without parallel imaging. The sequence used a scheme with six diffusion-weighted directions, b=600smm^{-2} plus one b≈0 (b_0) and 40 repetitions, averaged offline, giving an overall scan time of 30 minutes. A coronal oblique orientation was used with voxel size 1.17mmx1.17mmx4mm, We validated the sequence in 10 MS patients with a history of optic neuritis and 11 healthy controls: mean fractional anisotropy was reduced in the patients: 0.346(±0.159) versus 0.528(±0.123), p<0.001; radial diffusivity was increased: 0.940(±0.370)x10^{-6}mm^{2}s^{-1} compared to 0.670(± 0.221)x10^{-6}mm^{2}s^{-1} (p<0.01). No significant differences were seen for mean diffusivity or mean axial diffusivity.

KEY WORDS: 3T, diffusion, multiple sclerosis, optic nerve, optic neuritis

Introduction

The optic nerve is affected by neuroinflammatory diseases such as multiple sclerosis. As a discrete white matter tract providing sensitive measures of clinical function, it provides a useful model to study the pathophysiology of individual demyelinating lesions. Inflammatory demyelinated lesions in the optic nerve due to optic neuritis are pathologically identical to multiple sclerosis plaques observed elsewhere in the central nervous system (CNS) (Breij et al., 2008). *In vivo* measurement of the diffusion coefficient of water molecules in the optic nerve is of potential relevance for the study of focal demyelination and axonal loss in optic neuritis and multiple sclerosis (Schmierer et al., 2007; Song et al., 2005). Thus, abnormalities in quantitative diffusion tensor (DT)-derived parameters in the anterior visual pathway that can be related to clinical and electrophysiological measures of visual function can also be used to elucidate symptom pathophysiology and inform on disease mechanisms (Kolappan et al., 2009).

However, there are several challenges associated with DT imaging (DTI) of the optic nerve. Due to its small size there is a trade-off between high spatial resolution and adequate signal-to-noise ratio (SNR) [the diameter of the human optic nerve has previously been quoted to be 3-4mm (Xu et al., 2008) or 3-7mm (Wang et al., 2011)]. Tissue signal may be contaminated by signal from surrounding cerebrospinal fluid (CSF) and fat (Barker, 2001). Motion artifacts may result from involuntary motion of the nerve in addition to patient motion (Xu et al., 2008). Additionally, various issues may arise from the use of rapid imaging techniques such as echo planar imaging (EPI), in particular geometric distortions due to susceptibility differences of air, bone and tissue, and through-plane dephasing resulting in signal drop out.

Many artifacts in EPI result from the much smaller bandwidth per pixel (frequency difference between adjacent voxels) along the phase-encoding direction compared with the frequency-encoding axis. This means that chemically shifted signals from fat will be displaced by many pixels, and that small magnetic field differences (of the order of 1ppm) will result in much greater spatial distortion along the phase-encoding axis, due, for example, to susceptibility differences of air, bone and tissue. Such susceptibility-induced distortions become even more of a concern both at higher image resolution and higher magnetic field strengths. In fact, the field of view (FOV) in the phase-encoding direction for each echo-train readout and the time between the acquisition of two consecutive k-space lines both affect the bandwidth (which is proportional to 1/echo spacing), and therefore

the magnitude of image distortions. In order to minimize such distortions, the phase-encoding FOV for each echo-train readout may be reduced, for example, by using parallel imaging, thereby reducing the acquisition window duration and hence image distortions. However, this may not be available along all imaging axes, depending on the type of receiver coil used. Ramp sampling and a higher receiver bandwidth can also be used to reduce the echo spacing. The bandwidth in EPI is often set to the maximum possible (at a cost of a reduction in SNR) because distortions are such a problem with this technique (Skaare and Bammer, 2011). Alternatively, the pixel resolution could be reduced (although in the case of the optic nerve this is not a desirable option as, due to its small size, high resolution is required to avoid major partial volume issues), or multi-shot EPI could be used (although navigator echoes would then be required for motion correction between shots). For small objects such as the optic nerve, the echo train length could be reduced by reducing the FOV, however this may result in aliasing (wrap-around artifact), unless techniques such as ZOOM-EPI [e.g., (Hickman et al., 2005)] are employed. These techniques, however, are not available on all clinical scanners, including the one used in this study, and therefore a research agreement with the manufacturer and sequence programming efforts would be needed.

Based on the manufacturer's standard DTI sequence, we developed a multi-slice fat and CSF-suppressed DTI protocol in healthy controls to image both optic nerves simultaneously at 3T. This sequence was then tested by quantitative assessment of mean diffusivity (MD), fractional anisotropy (FA), axial diffusivity ($\lambda_{\parallel}$) (principal eigenvalue of the diffusion tensor), and radial diffusivity ($\lambda_{\perp}$) (average of second and third eigenvalues) in multiple sclerosis subjects with a history of optic neuritis.

Methods

This study was approved by the local ethics committee and all subjects provided informed consent in writing prior to the commencement of the data acquisition. Images were acquired on a Siemens MAGNETOM 3T Tim Trio scanner (Siemens Healthcare, Erlangen, Germany), using a body coil transmitter and a twelve-element receive head coil. Maximum gradient strength was 45 mT m^{-1} along z and 40 mT m^{-1} along x and y. Coronal oblique slices were planned using a separately acquired T_2-weighted sagittal image, as indicated in figure 1, with phase encoding in the superior/inferior (S/I) direction and signal saturation bands applied both superiorly and inferiorly to the prescribed imaging area to minimize wrap-around artifacts.

Sequence development in a healthy control

Two protocols, based on the standard (manufacturer's) DTI sequence were compared, one using parallel imaging [Generalised Autocalibrating Partially Parallel Acquisitions, GRAPPA (Griswold et al., 2002)] and the other without parallel imaging.

For protocol comparison, a healthy volunteer (female, age 26) was scanned. Coronal images were acquired using a spin echo (SE) EPI sequence with an inversion pulse for CSF suppression and a spectral-spatial excitation pulse for fat suppression. Both protocols had a diffusion scheme of six diffusion-weighted (DW) directions [(Gx, Gy, Gz) = (1, 0, 1), (-1, 0, 1), (0, 1, 1), (0, 1, -1), (1, 1, 0), (-1, 1, 0)], with b≈600smm^{-2} plus one b≈0smm^{-2} (b_0), and used at least 20 averages to enable definition of the central position of the optic nerve (Wheeler-Kingshott et al., 2002; 2000). Although for white matter diffusion acquisitions the optimal b-value is approximately 1000ms^{-2}, much lower b-values are typically used in optic nerve DTI studies [e.g. (Kolbe et al., 2009; Naismith et al., 2010; Techavipoo et al., 2009; Wheeler-Kingshott et al., 2002; 2006] in order to maximize SNR and because of the motion sensitivity of DTI and the constant motion of the optic nerve.

It has also previously been shown that, for optic nerve DTI, the acquisition of repeated averages of the same diffusion direction are necessary in order to minimize the effect of optic nerve motion between image acquisitions (Wheeler-Kingshott et al., 2000). This improves the delineation of the central position of the optic nerve, hence our choice to acquire multiple averages of data along only six diffusion directions, rather than a larger number of unique diffusion directions.

Two gradients were applied simultaneously with the maximum achievable amplitude for each to achieve the requested b-value whilst minimizing the echo time (TE). Sixteen contiguous 4mm slices were acquired, with FOV=15cm, acquisition matrix 128x64 (pixel size 1.17mmx1.17mm), TR=6s, TI=1.2s, TE=82ms. An initial starting point for the inversion time was selected based on the sequence signal equation (for the partic-

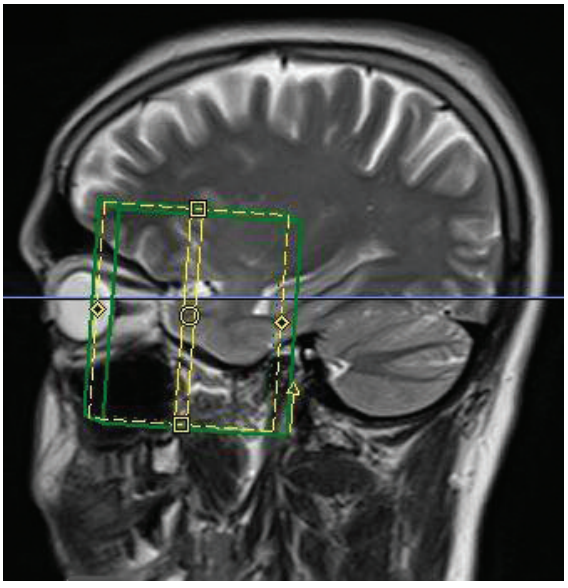

Figure 1 - Sagittal image of a single subject with the positions of the coronal slices through the optic nerve indicated.

ular TR value of the sequence), then iteratively optimized by altering the TI and choosing the value at which signal from CSF was effectively nulled.

(i) Parallel imaging – speed up factor 2

For this part of the testing, the protocol was run with an acceleration factor of 2 in the phase-encoding direction. Given that the geometry of the 12-element receive coil does not allow parallel imaging in the S/I direction, the phase-encoding direction was set as right to left (R/L). In order to evaluate the effect of geometrical distortions with reference to the optic nerves, the acquisition was run twice, each time with 20 repetitions, with the phase-encoding direction reversed (from R/L to L/R) in the second acquisition (Kolbe et al., 2009), giving a total scan time of 30 minutes. This procedure allowed the acquisition of usable data for each optic nerve (Kolbe et al., 2009). In fact, because of the spatial displacement due to the susceptibility distortions, applying gradients R/L obscured one optic nerve that ended up being very close to other tissue structures, while applying them L/R obscured the other optic nerve.

(ii) Standard acquisition:

Distortions present in the protocol using phase encoding in the R/L or L/R direction affected optic nerve identification, as stated in (i). We therefore set up a protocol applying the phase-encoding gradient in the S/I direction to alleviate this problem. However, this did not allow the use of GRAPPA (Griswold et al., 2002) due to the geometry of coil elements (parallel imaging could not be applied in the S/I direction).
Signal saturation bands were applied superiorly and inferiorly to the prescribed imaging area to minimize wrap-around artifacts, which would occur in the phase-encoding direction if the FOV were smaller than the head, causing the region beyond the desired area to project inside the image. This resulted in superior image quality and minimal artifacts compared to protocol (i). In order to compensate for the low SNR and to estimate the average position of the optic nerve, 40 averages were acquired as previously described at 1.5T (Wheeler-Kingshott et al., 2006), taking approximately 30 minutes in total.

Sequence validation in multiple sclerosis patients and controls

Ten subjects with secondary progressive multiple sclerosis (7M, 3F, age 40-54, mean age 48.4, SD 4.1 years) and 11 controls (7M, 4F, age 25-53, mean age 37.2, SD 8.8 years) were recruited. Sixteen (of twenty) eyes in the patient group had been affected by a previous clinical episode of optic neuritis 5-27 years prior to this study (Table I). Good recovery of visual function (defined as ≤0.1 logMAR) was seen in eight of the 16 affected eyes (mean logMAR: 0.15, range: -0.14 to 0.66). In all, we studied 16 clinically affected patients' optic nerves and four unaffected patients' optic nerves. All the optic nerves of the controls were included in the study. All the participants were imaged using the standard acquisition protocol (ii).

Image analysis

DTI analysis was performed using an established procedure (Trip et al., 2006; Wheeler-Kingshott et al., 2002). In order to reduce noise while preserving structure, a non-linear smoothing algorithm was applied prior to averaging (Parker et al., 2000). In order to define the central position of the optic nerve (Wheeler-Kingshott et al., 2002; 2000), and to ensure sufficient SNR, diffusion data were averaged to give seven DW volumes (one b_0 and six $b \approx 600 s mm^2$). The motion of the optic nerve was ''frozen'' during each single-shot acquisition of one image, however motion between successive acquisitions was problematic; averaging over many images was found to be the best way to allow for this, resulting in high quality images of the mean position of the nerve (Wheeler-Kingshott et al., 2000). The data were then eddy current corrected using the FSL software library (http://www.fmrib.ox.ac.uk/fsl), and the DT was fitted using the Camino software toolkit

Table I - Clinical details of optic neuritis patients included in the clinical study.

Pt	Age (yrs)	Gender	MS subtype	EDSS	Disease duration (yrs)	Optic nerve, side affected	Time elapsed since first clinical episode of optic neuritis (yrs)
01	44	M	SP	6.5	19	R	19
02	51	M	SP	6	26	Both	L-26, R-9
03	40	F	SP	6.5	13	Both	L-6, R-unknown*
04	48	M	SP	6	27	L	5
05	48	M	SP	6.5	11	Both	R-11, L-10
06	53	M	SP	6	18	R	18
07	53	F	SP	6.5	5	L	5
08	51	M	SP	5.5	7	Both	R-7, L-6
09	46	F	SP	6.5	11	Both	R-7, L-6
10	51	M	SP	6.5	6	Both	R-6, L-5

Abbreviations: SP=secondary progressive; EDSS=Expanded Disability Status Scale score; * Patient unsure of the exact time and not evident from clinical notes

(www.camino. org.uk) (Cook et al., 2006).
Small, square regions of interest (ROIs) of fixed size (2x2 voxels or 5.5mm^2) were manually placed on the b_0 averaged coronal oblique images using DispImage (Plummer, 1992), using the maximum signal intensity and minimum standard deviation to guide positioning. The ROIs were then applied to the calculated parameter maps to determine diffusion-related indices. Potential contamination of ROIs by CSF due to optic nerve atrophy was controlled for by the use of CSF suppression and the selection of small ROIs (2x2 voxels in total size). The MD, FA, $\lambda_{\parallel}$ and $\lambda_{\perp}$ were measured in each optic nerve of all volunteers. The direction of the principal eigenvector associated with $\lambda_{\parallel}$ was visually assessed according to the study by Wheeler-Kingshott and Cercignani (2009). These parameters were measured over multiple slices for all ROIs where the optic nerve could be reliably identified [average 3.5 (range: 3-6) consecutive slices in each nerve for both controls and patients in the validation study], and mean values were calculated from all measurements in both nerves.

Results

Sequence development in a healthy control

Averaged b_0 images acquired using protocol (i) with phase-encoding along the R/L direction and parallel imaging showed significant distortion artifacts (see Fig. 2; artifacts indicated by yellow arrows). In figure 2b, the phase-encoding direction was reversed with respect to 2a, and the direction of the distortion artifact was also reversed. By contrast, images acquired using protocol (ii) with the S/I phase-encoding direction allowed consistent location of the optic nerve position and reliable determination of DTI parameters. Example images acquired using protocol (ii) are shown in figure 3, with averaged b_0 images (a) at the top, and MD (b) and FA (c) images below; optic nerve positions are also indicated by red arrows.
A mean MD value of 1.07 (±0.10) x 10^{-6} m^2s^{-1} in the left optic nerve and 1.03 (±0.17) x 10^{-6} m^2s^{-1} in the

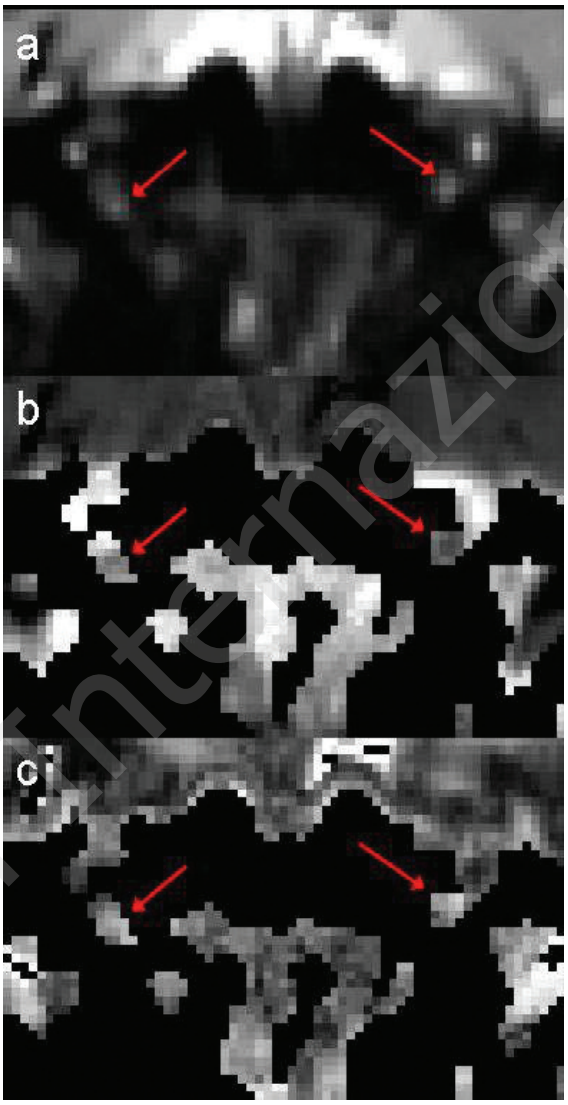

Figure 3 - Averaged b_0 (a), MD (b) and FA (c) images of the central slice of the optic nerve for a single subject, acquired using the standard high-resolution protocol, with the positions of the optic nerves indicated by red arrows.

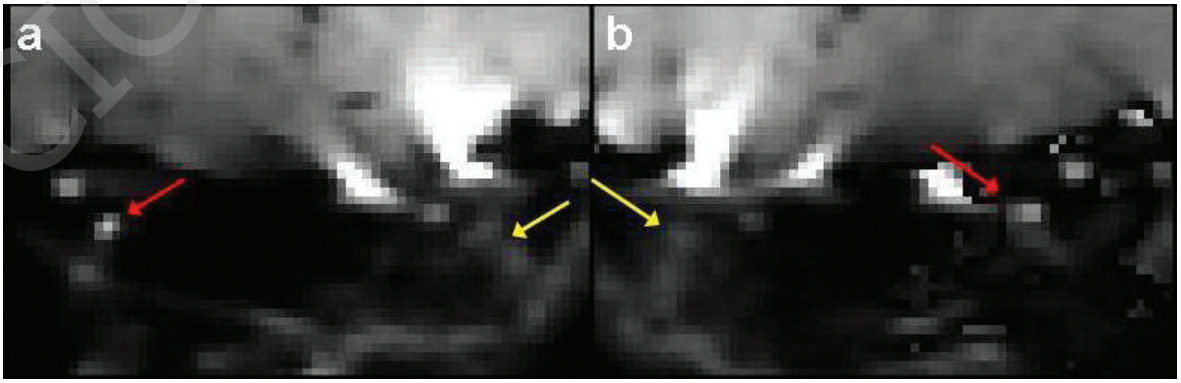

Figure 2 - Averaged b=0 (b_0) images for protocol (i); the phase-encoding direction is reversed in (b) compared to (a). Arrows indicate the position of the optic nerve (red) and distortion artifact (yellow).

right optic nerve was measured using the parallel imaging protocol (over four consecutive slices in each nerve, since the two nerves were imaged separately using this protocol). A mean value of 1.11 (±0.24) x 10^{-6} m^2s^{-1} was measured for the left optic nerve and 1.21 (±0.14) x 10^{-6} m^2s^{-1} for the right optic nerve using the standard acquisition protocol (ii) (over four consecutive slices).

The R/L distortions present in the images acquired with parallel imaging according to protocol (i) always resulted in one optic nerve being obscured (either the right or left optic nerve, depending on the phase-encoding direction - see Fig. 2), as previously demonstrated by Kolbe et al. (2009). Combining L/R and R/L data by using a distortion correction algorithm could be an option but would double the scan time making this approach non-clinically feasible. Some wrap-around occurs in the S/I direction in more posterior slices of volumes acquired using the standard acquisition protocol (ii) (see Fig. 3), but images are much less distorted in the R/L direction. By carefully positioning the coronal oblique slices and using S/I saturation bands, it is possible to ensure that the wrap-around does not overlap with the optic nerve, thus allowing diffusion parameters to be measured simultaneously in both nerves. Consequently, this approach was chosen for the clinical measurements.

Sequence validation in healthy controls and multiple sclerosis patients

A set of b_0 images for a control subject, acquired using the standard high-resolution protocol, are shown in figure 4, with the positions of the optic nerves and optic chiasm (blue) indicated by arrows (all averages combined, slice order: anterior to posterior). Figure 5 (over) shows averaged DW images (from anterior to posterior) for the same subject acquired using the same protocol (ii), with red arrows indicating the positions of the optic nerves, and a blue arrow indicating the optic chiasm. In both figures, the ROI positions (four pixels in size) are indicated in red.

Healthy control mean optic nerve MD and FA values measured using the standard acquisition protocol (ii) were consistent with previous measurements made at 1.5T (Chabert et al., 2005; Trip et al., 2006; Wheeler-Kingshott et al., 2006) and 3T (Kolbe et al., 2009; Naismith et al., 2009; 2010; Smith et al., 2011; Techavipoo et al., 2009; Wang et al., 2011; Xu et al., 2007). No significant R/L difference was observed in any diffusion parameter (tested by performing two-tailed paired Student's t-tests for the control group as a whole for each parameter); hence, averaged values are reported here.

One-way ANCOVA tests, with post-hoc paired comparisons were performed to test for significance of changes in patients' affected nerves compared to healthy control nerves, with gender and age included as covariates in the model. Mean FA was reduced in clinically affected nerves from the patient group compared to control nerves [0.346 (±0.159) vs 0.528 (±0.123), $p<0.01$]. We found no significant differences in mean MD between clinically affected and control nerves [1.14 (±0.36) x 10^{-6} mm^2s^{-1} vs 1.00 (±0.17) x 10^{-6} mm^2s^{-1}, $p=0.256$], or in mean $\lambda_{\parallel}$ [1.46 (±0.41) x 10^{-6} mm^2s^{-1} vs 1.57 (±0.25) x 10^{-6} mm^2s^{-1}, $p=0.509$].

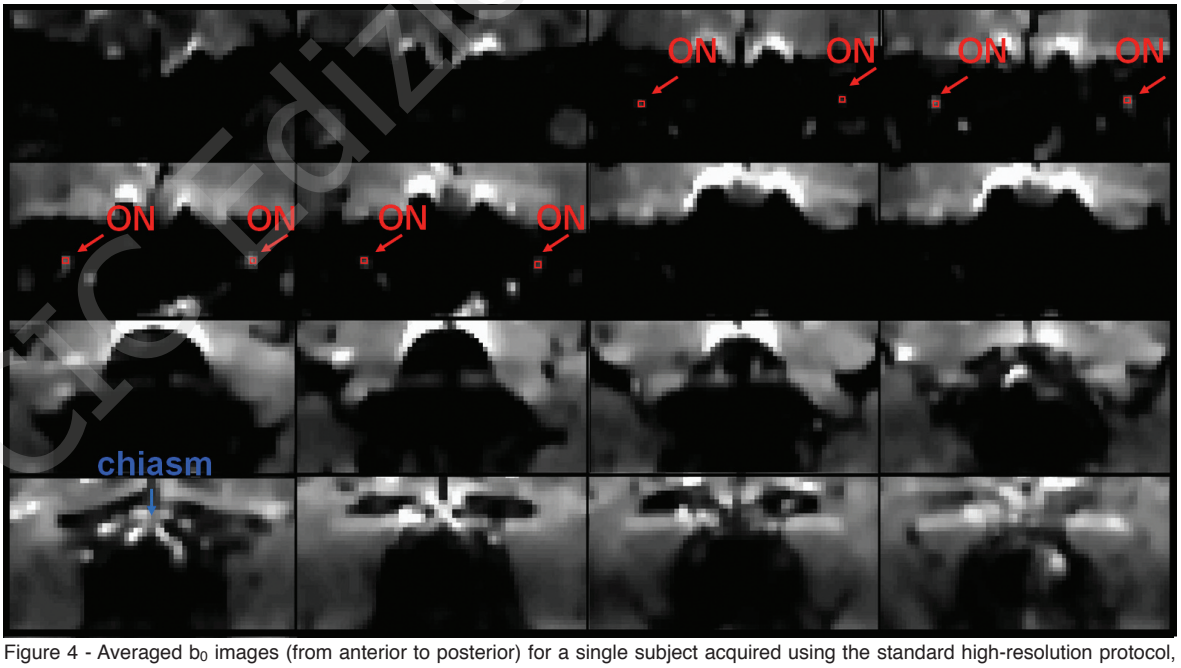

Figure 4 - Averaged b_0 images (from anterior to posterior) for a single subject acquired using the standard high-resolution protocol, with red arrows indicating the positions of the optic nerves, red indicating the positioning of the 4 pixels included in each of the ROIs, and a blue arrow indicating the optic chiasm. The anterior part of the optic nerve is easiest to observe, whereas its middle portion can become obscured due to the wrap-around artifact in posterior image slices.

Mean $\lambda_{\perp}$ for patients' affected nerves was significantly increased compared to the control mean value [0.94 (±0.37) x 10^{-6} mm^2s^{-1} vs 0.67 (±0.22) x 10^{-6} mm^2s^{-1}, $p<0.05$].

We performed one-way ANCOVA tests with post-hoc paired tests for comparisons (again including age and gender as covariates) of differences between both clinically affected nerves that recovered and those that did not, and also between recovered nerves and healthy control nerves. The only parameter that showed any difference between groups was FA: the FA of patients' recovered nerves was reduced to 0.346 (±0.179), in comparison with the mean control value of 0.528 (±0.123) ($p<0.05$).

Additionally, we performed exploratory correlations between the patients' logMAR visual scores and all the optic nerve DTI measures obtained. No significant correlations were found.

Discussion

Accurate diffusion measurements in the optic nerve may help to elucidate pathophysiological mechanisms in optic neuritis and other intrinsic optic nerve pathologies. However, optic nerve DTI is extremely challenging, and higher field strengths pose further problems despite the potentially increased SNR and resolution. Several approaches have been published, but many require unconventional pulse sequence design and hence sequence development (Dowell et al., 2009; Hickman et al., 2005; Koch et al., 2002; Naismith et al., 2009; Trip et al., 2006; Wheeler-Kingshott et al., 2002; Xu et al., 2007).

A recently published study described a 3T SE-EPI sequence with parallel imaging (acceleration factor 3) to acquire 10x3.5mm slices, with in-plane resolution 1.3mmx1.3mm, perpendicular to each nerve individually (Kolbe et al., 2009). Twenty-two averages were performed of an optimized six-direction scheme, with a b-value of 600s/mm^2. This approach required the DTI sequence to be performed twice, once for each nerve (with the phase-encoding direction reversed), due to geometric distortions in the R/L direction, and therefore doubled the scan time. Another approach was proposed by Andersson et al. (2003) to correct for susceptibility distortions in SE-EPI images; this required two sets of data: one acquired with the phase-encoding direction reversed, plus a B_0 map, however, it may not be feasible for application in the optic nerve.

Techavipoo et al. (2009) used a conventional single-shot SE-EPI protocol with parallel imaging factor 2.5 and additional field inhomogeneity maps covering the whole brain with a voxel size of 1.5mmx1.5mm, and 3mm slices, and found that optic nerve tractography became feasible with geometric distortion correction. However, DTI measures were not significantly different when calculated with or without the use of distortion correction. Diffusion-weighted images were acquired with directional resolution of 32 directions (but no averaging) and a b-value of 850 s/mm^2, and the DTI acquisition took nine minutes.

Wang et al. (2011) performed axial optic nerve DTI with parallel imaging factor 2, enhanced gradients to improve SNR, and a higher resolution (0.9mmx0.9mm, and 2mm slices) to decrease partial volume effects. They used a b-value of 1000s/mm^2, and 64 diffusion direc-

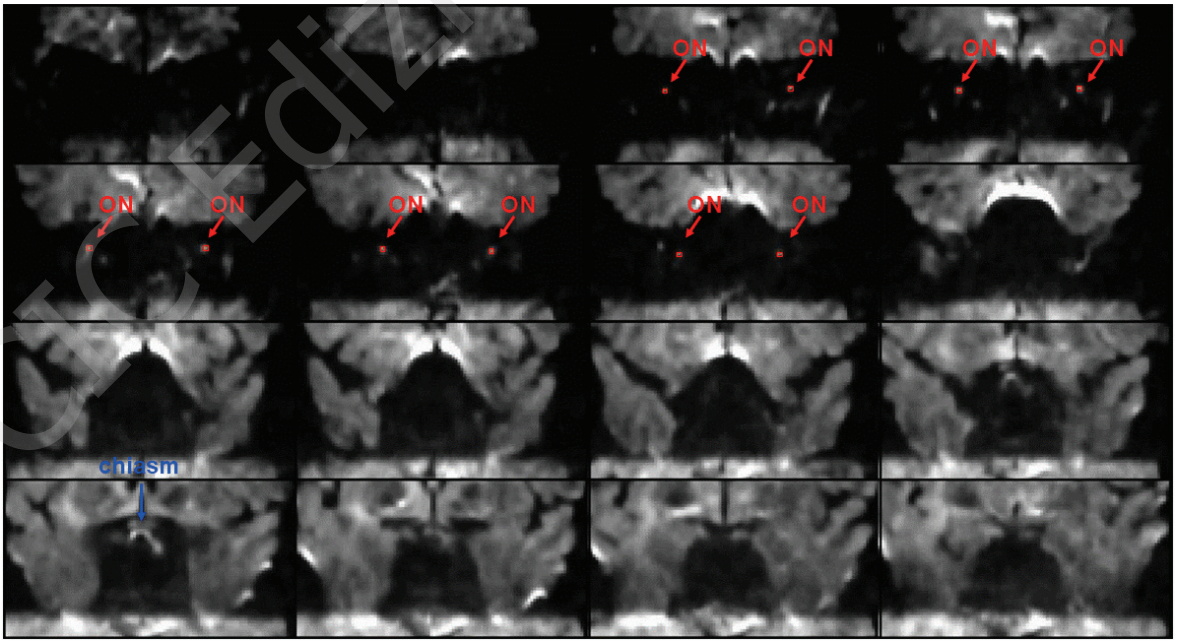

Figure 5 - Averaged diffusion-weighted images (from anterior to posterior) for a single subject acquired using the standard high-resolution protocol, with red arrows indicating the positions of the optic nerves, red indicating the positioning of the 4 pixels included in each of the ROIs, and a blue arrow indicating the optic chiasm.

tions, but did not apply CSF suppression in order to minimize acquisition time, therefore some contamination of signal from CSF may have occurred. The acquisition time was five minutes and 42 seconds.

Naismith et al. (2010) studied 70 subjects with a history of optic neuritis more than six months prior to examination, using a single-shot SE-EPI reduced-FOV technique with twice refocused diffusion weighting, fat suppression and cardiac gating. They acquired images with 1.3mm isotropic voxels in a total scan time of 40 minutes. Radial diffusivity was found to distinguish between healthy nerves and between unaffected and affected nerves in patients, as well as categories of visual recovery. Eight to 12 image sets, each with one b_0 and 12 DW images on 12 diffusion-encoding directions with b=600 s/mm^2 were acquired for each slice group. Total scan time was 40 minutes.

Smith et al. (2011) performed the largest 3T optic nerve DTI study of a cohort of multiple sclerosis patients (104 subjects), using a coronal-oblique SE-EPI sequence with outer volume suppression, and parallel imaging factor 3 to allow reduced TE; this gave a total scan time of just nine minutes and 22 seconds. The nominal acquired voxel size was 1.18mmx1.18mmx2.5 mm, and the data were zero-padded in *k*-space to achieve a reconstructed in-plane resolution of 0.28mmx0.28mm. A b-value of 500s/mm^2 was used, and 15 gradient directions uniformly distributed about a sphere, with five b_0 acquisitions, were performed. DTI measures were found to be sensitive to optic nerve damage.

In this study, we used a protocol with phase encoding in the S/I direction (in order to minimize artifacts caused by distortion and wrap-around) and without parallel imaging (due to the receive coil geometry) to image optic neuritis patients and healthy controls. Coronal-oblique DW images of both nerves were successfully acquired simultaneously at 3T, incorporating CSF and fat suppression to aid identification and delineation of the nerves. Averaging of magnitude images was then used to compensate for the low SNR in the acquired images and to estimate the average position of the optic nerve as previously described at 1.5T (Wheeler-Kingshott et al., 2006; 2000). Our protocol achieves a higher in-plane resolution than most of the above-mentioned studies [with the exception of the protocol used by Wang et al. (2011), in which 64 directions were acquired but no averaging was performed to determine the optic nerve position; and no CSF suppression was used] and simultaneous imaging of both nerves, with a higher number of averages than all the other previous studies used to optimally estimate the central optic nerve position. Unlike some of the studies mentioned (Naismith et al., 2010; Smith et al., 2011), our protocol was developed without the need for additional resources not likely to be available on standard clinical scanners, and can be readily implemented on any 3T system. We believe that the DTI sequence acquisition time (30 minutes) could be incorporated within a dedicated DTI study protocol.

A reduced FOV technique such as ZOOM DTI (Wheeler-Kingshott et al., 2002; 2006) – this has low sensitivity to motion and magnetic susceptibility artifacts – may be beneficial if available for optic nerve DTI at 3T without the need for additional pulse sequence programming, but this was not the case for this study. Unlike optic nerve DTI studies at 1.5T, Rayleigh noise correction was not necessary as the SNR of the b_0 images prior to averaging was typically around 10 (Miller and Joseph, 1993). Observed MD values were consistent with previous descriptions at 1.5T (Chabert et al., 2005; Trip et al., 2006; Wheeler-Kingshott et al., 2006) and 3T (Kolbe et al., 2009; Xu et al., 2007). FA values were slightly lower than in previous studies at 1.5T, however similar FA values have been described in a recent 3T study (Kolbe et al., 2009).

Results from studies in animal models suggest that DTI-derived axial and radial diffusivity reflect axonal loss and demyelination respectively (Song et al., 2005). In our study, mean radial diffusivity but not axial diffusivity was increased in nerves affected by previous optic neuritis compared to control nerves. This finding would thus be consistent with limited axonal loss and predominant demyelination in the affected nerves, and is also consistent with the findings in previous DTI studies of optic neuritis (Kolbe et al., 2009). Good visual recovery following optic neuritis, which was seen in all but one of our patients, is also consistent with limited axonal loss (Youl et al., 1991).

Further development and implementation of DTI in the optic nerves of patients with optic neuritis, and correlation of DTI measures with independent measures of visual function and conduction (VEPs) and retinal nerve fiber layer thickness seen using optical coherence tomography may enable the development of biomarkers of relevant pathological processes for use in experimental therapeutic studies, especially those focusing on neuroprotection and repair (Barkhof et al., 2009; Kolappan et al., 2009).

Despite the technical challenges of optic nerve DTI, we describe a protocol that does not require sequence development and can be implemented on any scanner. The acquisition time (30 minutes in total) could feasibly be accommodated in a dedicated DTI protocol. With careful slice positioning, simultaneous multi-slice DTI of both human optic nerves at 3T is feasible in a clinical setting, and the changes observed in the clinically affected nerves of optic neuritis patients demonstrate the sensitivity of the technique. The additional SNR and resolution available at higher field strengths and the advent of 32-channel coils may also reopen the question of the potential of parallel imaging methods for minimization of R/L distortions and faster acquisition times for optic nerve DTI.

Acknowledgments

The authors thank the Wellcome Trust and MS Society of Great Britain and Northern Ireland and the Medical Research Council for funding. This work was under-

taken at UCLH/UCL which received a proportion of the funding from the Department of Health's NIHR Biomedical Research Centres funding scheme.

References

Andersson JL, Skare S, Ashburner J (2003) How to correct susceptibility distortions in spin-echo echo-planar images: application to diffusion tensor imaging. Neuroimage 20:870-888.

Barker GJ (2001) Diffusion-weighted imaging of the spinal cord and optic nerve. J Neurol Sci 186 Suppl 1:S45-49.

Barkhof F, Calabresi PA, Miller DH, et al. (2009) Imaging outcomes for neuroprotection and repair in multiple sclerosis trials. Nat Rev Neurol 5:256-266.

Breij EC, Brink BP, Veerhuis R, et al. (2008) Homogeneity of active demyelinating lesions in established multiple sclerosis. Ann Neurol 63:16-25.

Chabert S, Molko N, Cointepas Y, et al. (2005) Diffusion tensor imaging of the human optic nerve using a non-CPMG fast spin echo sequence. J Magn Reson Imaging 22:307-310

Cook P A, Bai Y, Nedjati-Gilani S, et al. (2006) Camino: Open-source diffusion-MRI reconstruction and processing. In: Proceedings of the 14th Scientific Meeting of the International Society for Magnetic Resonance in Medicine. Seattle, WA, USA, Springer- Verlag

Dowell NG, Jenkins TM, Ciccarelli O, et al. (2009) Contiguous-slice zonally oblique multislice (CO-ZOOM) diffusion tensor imaging: examples of in vivo spinal cord and optic nerve applications. J Magn Reson Imaging 29:454-460.

Griswold MA, Jakob PM, Heidemann RM, et al. (2002) Generalized autocalibrating partially parallel acquisitions (GRAPPA). Magn Reson Med 47:1202-1210.

Hickman SJ, Wheeler-Kingshott CA, Jones SJ, et al. (2005) Optic nerve diffusion measurement from diffusion-weighted imaging in optic neuritis. AJNR Am J Neuroradiol 26:951-956.

Koch MA, Glauche V, Finsterbusch J, et al. (2002) Distortion-free diffusion tensor imaging of cranial nerves and of inferior temporal and orbitofrontal white matter. Neuroimage 17 :497-506.

Kolappan M, Henderson AP, Jenkins TM, et al. (2009) Assessing structure and function of the afferent visual pathway in multiple sclerosis and associated optic neuritis. J Neurol 256 :305-319.

Kolbe S, Chapman C, Nguyen T, et al. (2009) Optic nerve diffusion changes and atrophy jointly predict visual dysfunction after optic neuritis.Neuroimage 45:679-686.

Miller AJ, Joseph PM (1993) The use of power images to perform quantitative analysis on low SNR MR images. Magn Reson Imaging 11:1051-1056.

Naismith RT, Xu J, Tutlam NT, et al. (2009) Disability in optic neuritis correlates with diffusion tensor-derived directional diffusivities. Neurology 72:589-594.

Naismith RT, Xu J, Tutlam NT, et al. (2010) Radial diffusivity in remote optic neuritis discriminates visual outcomes. Neurology 74:1702-1710.

Parker GJ, Schnabel JA, Symms MR, et al. (2000) Nonlinear smoothing for reduction of systematic and random errors in diffusion tensor imaging. J Magn Reson Imaging 11 :702-710.

Plummer DL (1992) DispImage: a display and analysis tool for medical images. Revista di Neuroradiologica 5:489-495.

Schmierer K, Wheeler-Kingshott CA, Boulby PA, et al. (2007) Diffusion tensor imaging of post mortem multiple sclerosis brain. Neuroimage 35:467-477.

Skaare ST, Bammer R (2011) EPI-based pulse sequences for diffusion tensor MRI. In: Jones DK (Ed) Diffusion MRI: Theory, Methods, and Applications, Oxford: Oxford University Press, pp. 182-202.

Smith SA, Williams ZR, Ratchford JN, et al. (2011) Diffusion tensor imaging of the optic nerve in multiple sclerosis: association with retinal damage and visual disability. AJNR Am J Neuroradiol 32:1662-1668.

Song SK, Yoshino J, Le TQ, et al. (2005) Demyelination increases radial diffusivity in corpus callosum of mouse brain. Neuroimage 26:132-140.

Techavipoo U, Okai AF, Lackey J, et al. (2009) Toward a practical protocol for human optic nerve DTI with EPI geometric distortion correction. J Magn Reson Imaging 30:699-707.

Trip SA, Wheeler-Kingshott C, Jones SJ, et al. (2006) Optic nerve diffusion tensor imaging in optic neuritis. Neuroimage 30:498-505.

Wang MY, Qi PH, Shi DP (2011) Diffusion tensor imaging of the optic nerve in subacute anterior ischemic optic neuropathy at 3T. AJNR Am J Neuroradiol 32:1188-1194.

Wheeler-Kingshott CA, Cercignani M (2009) About "axial" and "radial" diffusivities. Magn Reson Med 61:1255-1260.

Wheeler-Kingshott CA, Trip SA, Symms MR, et al. (2006) In vivo diffusion tensor imaging of the human optic nerve: pilot study in normal controls. Magn Reson Med 56:446-451.

Wheeler-Kingshott CA, Parker GJ, Symms MR, et al. (2002) ADC mapping of the human optic nerve: increased resolution, coverage, and reliability with CSF-suppressed ZOOM-EPI. Magn Reson Med 47:24-31.

Wheeler-Kingshott CA, Ciccarelli O, Parker GJ, et al. (2000) Quantification of the motion of the optic nerve. In: Proceedings of the Annual Meeting of the European Society of Magnetic Resonance in Medicine and Biology (ESMRMB). Paris, Springer-Verlag

Xu J, Naismith RT, Trinkaus KM, et al. (2007) Towards accurate in vivo diffusion measurement in human optic nerve. In: Proceedings of the 15th Annual Meeting of the International Society for Magnetic Resonance in Medicine. Berlin, Germany, Curran Associates, Inc.

Xu J, Sun SW, Naismith RT, et al. (2008) Assessing optic nerve pathology with diffusion MRI: from mouse to human. NMR Biomed 21:928-940.

Youl BD, Turano G, Miller DH, et al. (1991) The pathophysiology of acute optic neuritis. An association of gadolinium leakage with clinical and electrophysiological deficits. Brain 114:2437-2450.